HHS Public Access

Author manuscript

Nat Genet. Author manuscript; available in PMC 2015 April 01.

Published in final edited form as:

Nat Genet. 2014 October ; 46(10): 1135–1139. doi:10.1038/ng.3066.

Mutation of *NLRC4* causes a syndrome of enterocolitis and autoinflammation

Neil Romberg[#1], **Khatoun Al Moussawi**[#2], **Carol Nelson-Williams**[3,4], **Amy L Stiegler**[5], **Erin Loring**[3], **Murim Choi**[3,4], **John Overton**[3], **Eric Meffre**[2,6], **Mustafa K Khokha**[1,3], **Anita J Huttner**[7], **Brian West**[7], **Nikolai A Podoltsev**[2], **Titus J Boggon**[5], **Barbara I Kazmierczak**[2,8,**], and **Richard P Lifton**[2,3,4,**]

[1]Department of Pediatrics, Yale University School of Medicine, 333 Cedar Street, New Haven, Connecticut 06510, USA

[2]Department of Internal Medicine, Yale University School of Medicine, 330 Cedar Street, New Haven, Connecticut 06510, USA

[3]Department of Genetics, Yale University School of Medicine, 333 Cedar Street, New Haven, Connecticut 06510, USA

[4]Howard Hughes Medical Institute, Yale University School of Medicine, 295 Congress Avenue, New Haven, Connecticut 06510, USA

[5]Department of Pharmacology, Yale University School of Medicine, 333 Cedar Street, New Haven, Connecticut 06510, USA

[6]Department of Immunobiology, Yale University School of Medicine, 300 Cedar Street, New Haven, Connecticut 06510, USA

[7]Department of Pathology, Yale University School of Medicine, 310 Cedar Street, New Haven, Connecticut 06510, USA

[8]Department of Microbial Pathogenesis, Yale University School of Medicine, 295 Congress Ave, New Haven, Connecticut 06520, USA

[#] These authors contributed equally to this work.

Abstract

[**]These authors jointly directed this work. Correspondence should be addressed to R.P.L. (richard.lifton@yale.edu), or B.I.K. (barbara.kazmierczak@yale.edu)..

AUTHOR CONTRIBUTIONS

R.P.L, B.I.K. N.R. and K.A. designed the study and experiments. K.A. and N.R. performed cellular and molecular experiments. N.R., N.A.P., M.K.K. and E.L. identified, consented, recruited study subjects and provided clinical information. B.W. and A.J.H. provided autopsy/biopsy interpretations and images. C.N.W., J.O. and M.C. generated and analyzed sequencing data. T.J.B. and A.L.S. generated and interpreted three-dimensional mutation maps of NLRC4. N.R. and E.M. processed patient samples. N.R., R.P.L and B.I.K. wrote the manuscript.

SUPPLEMENTAL MATERIALS

Six supplementary figures and **three** supplementary tables are available.

COMPETING FINANCIAL INTERESTS

The authors declared no competing financial interests.

Upon detection of pathogen-associated molecular patterns, innate immune receptors initiate inflammatory responses. These receptors include cytoplasmic NOD-like receptors (NLRs), whose stimulation recruits and proteolytically activates caspase-1 within the inflammasome, a multi-protein complex. Caspase-1 mediates the production of interleukin-1 family cytokines (IL1FCs), leading to fever, and inflammatory cell death (pyroptosis)[1,2]. Mutations that constitutively activate these pathways underlie several autoinflammatory diseases with diverse clinical features[3]. We describe a family with a previously unreported syndrome featuring neonatal-onset enterocolitis, periodic fever, and fatal/near-fatal episodes of autoinflammation caused by a *de novo* gain-of-function mutation (p.V341A) in the HD1 domain of *NLRC4* that co-segregates with disease. Mutant NLRC4 causes constitutive Interleukin-1 family cytokine production and macrophage cell death. Infected patient macrophages are polarized toward pyroptosis and exhibit abnormal staining for inflammasome components. These findings describe and reveal the cause of a life-threatening but treatable autoinflammatory disease that underscores the divergent roles of the NLRC4 inflammasome.

Secretion of IL1FCs (IL-1 and IL-18) normally requires two signals. “Signal 1”, from membrane-spanning receptors (e.g. toll-like), induces expression of pro-IL1FCs[2]. “Signal 2”, from cytosolic detectors including NOD-like receptors (NLRs), leads to pro-caspase-1 autoproteolysis and activation[1]. Cleaved caspase-1 converts pro-IL-1 cytokines into their active forms[2,4]. One NLR, NLRC4, cooperates with NAIP to detect flagellin or components of the type three secretion system (TTSS), used by *S. typhimurium* and *P. aeruginosa* to infect host cells[5,6]. Upon ligand binding, NAIP and NLRC4 oligomerize and recruit the adaptor protein ASC (apoptosis associated speck-like protein containing a CARD)[7,8]. This macromolecular (>1 μm diameter) NLRC4 inflammasome induces autoproteolysis of pro-caspase-1 with subsequent IL1FC secretion and pyroptosis[1,7]. Mutant mice that cannot co-localize ASC and cleaved caspase-1 lose cytokine secretion yet retain pyroptosis.[6,9,10]

The index patient (**Fig. 1a**, III.3) presented at one week of life with secretory diarrhea and fever (38.8°C); no infectious cause was identified. Markers of systemic inflammation were elevated, including ferritin (4,840 ng/ml; nl 18-370 ng/ml) (**Fig. 1d**) and C-reactive protein (**Supplementary Table 1**). Natural killer cells (NK cells) were reduced. Hypertriglyceridemia, hypofibrinoginemia, coagulopathy and pancytopenia developed, culminating in death on day 23 from diffuse alveolar hemorrhage. Autopsy revealed splenomegaly, numerous activated ($CD163^+$) macrophages infiltrating the central nervous system (**Supplementary Fig. 1)** and widespread bowel autolysis. Remaining intestinal tissue showed mixed inflammatory cells and villous blunting (**Fig. 1b,** upper panel).

Two days after the index patient's funeral, his 43-year-old father (**Fig. 1a,** patient II.3) presented with fever (40.6 °C), acute respiratory distress syndrome, subarachnoid hemorrhage and hematochezia; disseminated intravascular coagulation and pancytopenia developed, with elevated ferritin (29,200 ng/ml), IL-18 (11,934 pg/ml; nl 69-503 pg/ml), C-reactive protein and soluble IL-2R (**Supplementary Table 1**). Bone marrow biopsy showed erythro- and myelophagocytosis (**Fig. 1c**). Ultrasonography revealed splenomegaly. NK-cell lymphopenia was prominent. As no infectious agent was isolated, high-dose intravenous immunoglobulin, dexamethasone and cyclosporine were instituted for immunosuppression.

He gradually improved and was discharged after 9 weeks, remaining on cyclosporine; serum ferritin normalized but IL-18 remained markedly elevated (**Fig. 1d,e**). He subsequently reported a lifelong history of periodic fevers (>40 °C) provoked by physical and emotional stressors. During infancy he had an extended hospitalization for fever, vomiting, non-bloody diarrhea and failure to thrive; no specific diagnosis was made. His gastrointestinal symptoms resolved by one year. In adulthood erythematous plaques and joint pains accompanied fevers; sero-negative psoriatic arthritis was diagnosed.

The father's family history revealed healthy parents and two additional offspring, one without illness and a five-year-old half-brother (III.2) of the deceased infant (III.3) who also had periodic fevers (range 38.9 - 40 °C) beginning on day three of life after circumcision. A more severe febrile episode associated with vomiting, non-hemolytic anemia and acute renal failure occurred at 6-weeks of age (**Supplementary Table 1**). Later his fevers were induced by over-exertion and accompanied by abdominal pain. A duodenal biopsy in the first year revealed villous blunting and intraepithelial lymphocytes (**Fig. 1b**, lower panel). Inflammatory markers including ferritin (516-856 ng/ml), C-reactive protein, soluble IL-2R and plasma IL-18 (11,520 to 24,129 pg/ml) were persistently elevated (**Fig. 1d,e)**. NK cells, normal in number, were dysfunctional by chromium release assays (**Supplementary Table 1**). Clinical signs of chronic inflammation included short stature (< 3rd percentile for height and weight) and recurrent myalgias.

During the index case's acute illness, the possibility of a novel genetic syndrome was considered, leading to exome sequencing of the index case and his parents (see Methods). Clincial features suggesting hemophagocytic lymphohistiocytosis led to examination of genes implicated in this syndrome[11]; no rare variants were identified (**Supplementary Table 2**). Upon the father's illness, 34 novel protein-altering variants (absent in dbSNP, 1000 genomes, NHLBI and Yale exome databases) shared by the index case and his father were identified, including six occurring at positions invariant among orthologs (**Supplementary Table 3**). While none of these altered genes causing known inflammatory diseases, one was in *NLRC4,* which encodes a core inflammasome protein. This p.Val341Ala variant occurs within helical domain 1 (HD1), which provides a ‘lid’ to the ADP nucleotide-binding domain (NBD) in the crystal structure of inactive NLRC4 **(Fig. 2).** Ligand binding normally opens this structure, leading to exchange of ATP for ADP, promoting oligomerization and inflammasome assembly[12]. Gain-of-function mutations in the NBD of the related protein NLRP3 cause constitutive NLRP3 inflammasome assembly, resulting in production of IL-1β, fever and a spectrum of autoinflammatory disorders, the cryopyrinopathies[13-15]. These diseases are clinically distinct from the disease in our family as the cryopyrinopathies lack gastrointestinal pathology[16].

Evaluation of *NLRC4*^{V341A} in the extended family demonstrated that it occurred *de novo* in the affected father, and co-segregated with the inflammatory disease **(Fig. 1a**). None of the other five novel variants at conserved positions showed co-segregation with disease or de novo mutation. The finding of a *de novo* mutation in NLRC4, that co-segregates with a consistent clinical syndrome and biomarkers of inflammasome activation, provides strong evidence that *NLRC4*^{V341A} causes this syndrome (syndrome of enterocolitis and autoinflammation associated with mutation in *NLRC4*; SCAN4).

To evaluate the consequence of NLRC4^{V341A}, we co-transfected wildtype or mutant human *NLRC4* into HEK293 cells with human *ASC* and *CASP1* and measured cleavage of procaspase-1. As anticipated, cleavage of pro-caspase-1 was ASC-dependent (**Fig. 3a**)[6]. Compared to *NLRC4^{WT}*, cells expressing *NLRC4^{V341A}* showed 4-fold increased spontaneous production of caspase-1 p35 (P=0.004; **Fig. 3a**). Assembled inflammasomes form discrete foci in cells. We counted GFP-tagged ASC foci in cells expressing NLRC4^{WT} or NLRC4^{V341A}. These foci were more frequently present in mutant than wildtype cells (12.3% versus 7.6%; P<0.0001) (**Fig. 3b**). Multiple ASC foci were not observed in any transfected HEK293 cells.

We investigated constitutive NLRC4 inflammasome activation in macrophages derived from peripheral blood monocytes of SCAN4 patients (II.3 and III.2) and healthy related (n=1) and unrelated (n=4) controls. Without a "signal 2" (i.e., NLR ligand), control macrophages did not form ASC foci nor did they stain with biotin-YVAD-FMK (which binds activated caspase-1; **Supplementary Fig. 2a,b**). In contrast, 3.3% of SCAN4 macrophages spontaneously formed ASC foci and 25.9% showed biotin-YVAD-FMK staining, similar to *NLRC4^{V341}*- transfected HEK293 cells (**Supplementary Fig.2 a,b and Fig. 3b**).

We cultured patient-derived or healthy donor macrophages for 18 hours with "signal 1" provocation (1 ng/ml LPS). As expected, without a "signal 2", healthy control macrophages showed no detectable secretion of IL-1β (<1.4 pg/ml) and small amounts of IL-18 (22 pg/ml). In contrast, macrophages from both SCAN4 patients (II.3 and III.2) secreted markedly increased IL-1β (76 pg/ml) and IL-18 (212 pg/ml) (P<0.0001 vs. controls for both; **Fig. 4a**).

We measured cell death-associated LDH release in the same 18-hour culture supernatants. SCAN4 macrophages released more LDH than healthy control macrophages (12.3% versus 4.7% P<0.0001) (**Fig. 4b**). Addition of Z-YVAD-FMK, which inhibits the catalytic site of cleaved caspase-1, significantly reduced IL-1 family secretion, but did not reduce cell death (**Supplementary Fig. 3a,b**). Thus NLRC4^{V341A} is gain-of-function, eliminating the requirement for "signal 2" for activation of caspase-1 and production of IL1FCs. NLRC4^{V341A} also promotes pyroptosis independent of caspase-1 cytokine processing.

We next infected LPS-primed healthy control or patient macrophages with either of two flagellated, TTSS-positive pathogens, *S. typhimurium* (strain SL1344) or *P. aeruginosa* (strain PAKΔSTY), thus providing both 'signal 1' and 'signal 2' provocation. As anticipated, LPS-primed healthy control macrophages secreted abundant IL1FCs and initiated pyroptosis upon infection (**Supplementary Fig. 4a,b**). Responses were reduced when infected with *P. aeruginosa* strain PAKΔ*popD*, which lacks a functional TTSS (**Supplementary Fig. 4a,b**). In contrast, SCAN4 macrophages secreted significantly less IL1FCs upon infection with pathogenic strains, yet showed more cell death than healthy control macrophages (**Supplementary Fig. 4a,b**).

Infected macrophages form inflammasomes microscopically identifiable as ASC foci which co-localize with caspase-1. Consistent with published reports using murine macrophages[9,17] we found that 93% of *S. typhimurium*-infected and 97% of PAKΔSTY-infected healthy control macrophages formed 1-3 large diameter (>1 μm) ASC foci (**Fig. 5a**, **left panel,** and

b and **Supplementary Fig. 5a**, **left panel**, and **b**). Most *S. typhimurium* (71%) or PAKΔSTY (67%)-infected cells with 1-3 ASC foci showed caspase-1 proteolysis, indicated by diffuse cytoplasmic biotin-YVAD-CMK staining (**Fig. 5a**, **left panel,** and **c** and **Supplementary Fig. 5a**, **left panel**, and **c**). Consistent with previous reports,[17,18] ASC foci in most *S. typhimurium* infected cells from healthy donors colocalized with aggregates of activated caspase-1 (**Supplementary Fig. 6)**. A small percentage of healthy donor cells (1.1% of *S. typhimurium*-infected control macrophages), had >6 ASC foci per cell; 93% of these stained with biotin-YVAD-FMK (**Fig. 5a**, **left panel,** and **c**). In PAKΔSTY-infected cells, none had >6 ASC foci (**Supplementary Fig. 5a**, **left panel**, and **c**). In contrast, SCAN4 macrophages showed more frequent cells with >6 ASC foci (6.8% for *S. typhimurium*-infected and 5.6% for PAKΔSTY-infected macrophages, each P<0.0001 vs. controls). Rare macrophages had more than 20 ASC foci (**Fig. 5a**, **right panels,** and **b** and **Supplementary Fig. 5a**, **right panels**, and **b**). Caspase-1 activation was generally limited in infected SCAN4 macrophages. Even in macrophages displaying >6 foci, only 50% infected with *S. typhimurium* and 44% infected with PAKΔSTY displayed diffuse cytoplasmic biotin-YVADCMK staining (P<0.0001 and P=0.0012 vs wildtype, respectively) (**Fig. 5a**, **right panels**, and **c** and **Supplementary Fig. 5**, **right panels**, and **c**). In contrast to wildtype cells, ASC foci in *S. typhimurium* infected SCAN4 cells did not colocalize with aggregates of activated caspase-1 (**Supplementary Fig. 6**). Lastly, ASC foci in biotin-YVAD-CMK negative macrophages were significantly smaller than in biotin-YVAD-CMK positive cells in both healthy controls and SCAN4 patients (**Fig. 5d** and **Supplementary Fig. 5d**).

These findings describe a previously unreported Mendelian autoinflammatory syndrome featuring periodic fever, neonatal-onset enterocolitis and high levels of IL1FCs, and demonstrate its causation by a gain-of-function mutation in *NLRC4*. Like NLRP3 cryopyrinopathies[14], SCAN4 is associated with constitutive activation of caspase-1 and production of IL1FCs. In the inhibited, ADP-bound state, Val341 of NLRC4 makes van der Waals contacts with side chains of an adjacent helix in the HD1 domain, comprising the 'lid' on the nucleotide-binding site. The decreased hydrophobicity of the Ala341 mutation may reduce this interaction, allowing more movement of helix α12 and promoting ATP for ADP exchange, either by favoring the open conformation of NLRC4, or by disrupting the stabilizing interaction of His443 with the beta-phosphate of ADP (**Fig. 2**). Either possibility would promote ligand-independent activation of NLRC4. It is compelling that Canna *et al.* have identified an independent *de novo* mutation in NLRC4, p.Thr337Ser[19]. The identification of two de novo mutations in close proximity in the same gene that segregate with a novel clinical phenotype provides strong support for a causal relationship of the mutations to disease pathogenesis.

SCAN4 is distinctive from NLRP3 cryopyrinopathies in its association with neonatal-onset enterocolitis. This may relate to *NLRC4* being highly expressed in intestinal macrophages while *NLRP3* is not[20]. It is interesting that the marked enterocolitis of each surviving SCAN4 patient resolved by one year of age. We speculate that this chronic inflammatory state may be exacerbated in the infant gut by constant "signal 1" provocation from newly acquired symbionts. As host-microbe interactions mature, a less pro-inflammatory microflora may account for reduced gut inflammation[21].

IL-1β - targeted drugs are approved for treatment of NLRP3 cryopyrinopathies[22-24]. We expect IL-1β blockade will be similarly effective in SCAN4 patients. Although both surviving members in our family have presently declined interictal therapy, the complementary report by Canna *et al* provides evidence for efficacy of IL-1 receptor blockade[19].

SCAN4 macrophages show high IL1FC secretion and increased cell death with "signal 1" despite the absence of "signal 2"; addition of "signal 2" frequently produces multiple ASC foci with increased cell death, despite blunted IL1FC secretion. One possible explanation is that mutant NLRC4 promotes traditional inflammasome assembly in the absence of "signal 2" provocation but intracellular ligand binding promotes formation of ASC foci that lack activated caspase-1, resulting in smaller structures with impaired ability to produce cytokines. This proposal is supported by mice with mutated inflammasome components[6,9,10] which demonstrate defective cytokine processing yet intact pyroptosis . Modulating the balance between cytokine production and pyroptosis may determine the distinct states of subclinical autoinflammation, periodic fever, and fatal or near-fatal autoinflammation seen in SCAN4 patients.

ONLINE METHODS

Research Subjects

The study protocol was approved by the Yale Human Research Protection Program. Informed consent was provided by all participants or their legal guardians. Clinical data was abstracted from medical records. Tissues from biopsy and autopsy specimens were labeled using standard hematoxylin and eosin staining protocols or by immunohistochemical staining with an anti-CD163 antibody (Abcam).

Genetic analysis

DNA was prepared from venous blood samples of the index case and kindred members. Exome sequencing of the index case and his parents was performed by capture on the NimbleGen 2.1 Exome reagent followed by 74 base paired end sequencing on the Illumina platform to high coverage (each targeted base was read by a mean of more than u80 independent reads in each subject) as previously described26. Sequences were aligned to NCBI Build 36 of the human genome and SNV and indel calls were assigned quality scores (QS) using SAMtools and annotated for novelty (using Yale, 1000 genomes, and NHLBI exome databases), for impact on encoded proteins, and for conservation of variant position as previously described26. Variants were sought in genes implicated in hemophagocytic lymphohistiocytosis; none were identified (**Supplementary Table 2**). Thirty-four protein-altering variants that were absent in dbSNP, 1000 genomes, NHLBI and Yale exome databases that were shared by the index case and affected father were identified (**Supplementary Table 3**) and evaluated. Only one was in a gene known to play a role in activation of the innate immune system (NLRC4). Variants in NLRC4 and the other 5 genes in which novel variants that occurred at completely conserved positions (ALK, DCC, FBXO4, KIF13B, and SLC7A6OS) were confirmed by PCR amplification followed by Sanger sequencing and transmission through the complete pedigree was evaluated. The

NLRC4 variant proved to be de novo in the affected father and perfectly cosegregated with the autoinflammatory syndrome in the pedigree, while the others were all transmitted from an unaffected grandparent of the index case and did not co-segregate with disease. The NLRC4 p.Val341Ala mutation has been deposited into the National Center for Biotechnology Information's ClinVar database (ClinVar accession #, SCV000172282)

Functional analysis of V341A altered NLRC4

NLRC4 activity was analyzed in HEK293-cells. Wild-type human NLRC4 was cloned into pMycB (Santa Cruz Biotech) and verified by Sanger sequencing. The c.1022 T->C mutation was introduced by site-directed mutagenesis (Stragene QuikChange) and verified by Sanger sequencing. Mutated and wildtype myc-*NLRC4* were transiently transfected into HEK293 cells along with N-terminal FLAG-human pro-caspase-1 and GFP-tagged human ASC using Lipofectamine2000 (Invitrogen). NLRC4 activity was visually measured 30h after transfection by spontaneous formation of GFP-ASC foci (as visualized in live cells by epifluorescent microscopy). Manual enumeration of ASC foci^{+} was performed over 20 representative fields at 20x magnification. Pro-caspase-1 p45 autoproteolysis was measured directly by western blotting for p35 (anti-FLAG M2 (F1804), 1:1000; Sigma) and p10 fragments (anti-caspase-1 p10 (sc-514), 1:200; Santa Cruz Biotech), using anti-mouse IgG-HRP or anti-rabbit IgG-HRP (Biorad) and enhanced chemiluminescence. The presence of NLRC4 and actin in lysates was confirmed by blotting with anti- c-Myc antibodies (9E10, 1:1000; Enzo Life Sciences) or anti-rabbit pan-actin polyclonal antibody (#4970, 1:5000; Cell Signaling Technology), respectively.

Functional studies of monocyte derived macrophages

CD14^{+} monocytes were purified from peripheral blood mononuclear cells of SCAN4 patients and healthy donor controls using anti-human CD14 magnetic beads (Miltenyi). Cells from the two living SCAN4 patients were used for all functional studies whereas the number and relatedness of healthy donors used varied from experiment to experiment and was based upon same-day availability. Monocytes were differentiated to macrophages in RPMI containing 10% FBS and M-CSF (10ng/ml) over 7 days[27]. 2×10^5 macrophages were cultured for 18 hours in culture media containing LPS (1ng/ml) with or without Z-YVAD-FMK (Enzo Life Sciences) at 0.1-0.5μM concentrations. Culture supernatants were collected and cells washed and re-cultured with LPS free media before infection with *P. aeruginosa* or S. *typhimurium*. PAKΔSTY and SL1344 are flagellated strains that are type 3 secretion system (T3SS)-positive. PAKΔ*popD* is a Fla+ strain that does not express a functional T3SS. Construction and characterization of bacterial strains has been previously described[6,28]. Infected macrophage culture supernatants were collected after one hour. Secreted IL-1β and IL-18 were measured by ELISA (Millipore and MBL, respectively) in both the 18-hour and one-hour culture supernatants. Cell-free LDH was measured according to manufacturer's protocol (Takara). LDH release in supernatants was normalized to LDH released from macrophages lysed with Triton X-100 (0.1%).

Immunofluoresence microscopy of infected macrophages

2×10^5 macrophages, differentiated as above, were plated on glass coverslips. Cells were incubated with 2 μM biotin-YVAD-CMK for 30 minutes prior to infection with *P. aeruginosa* PAKΔSTY or Δ*popD* or S. *typhimurium* SL1344 at a multiplicity of infection of 20 bacteria/cell for 1 hour. Cell were fixed with paraformaldehyde (4%), blocked with 1% fish scale gelatin (Sigma) in PBS + 0.1% TX-100, and stained with rabbit anti-ASC (AL177; AdipoGen) and 4',6-Diamidino-2-phenylindole (Sigma). A streptavidin-Alexa Fluor 488 conjugate (Invitrogen) and anti-rabbit Alexa Fluor 594 antibody (Life Technologies) were used for secondary stainings. Macrophages were visually inspected for immunofluorescence using an Axiovert 200M microscope. Manual enumeration of ASC^+ and $YVAD^+$ macrophages was performed over 20 representative fields at 20x magnification. DAPI staining of bacterial DNA was used to confirm macrophage infection. High detail magnification for phased images at 60X and 100X was performed on a Nikon Eclipse TE2000-S microscope.

Supplementary Material

Refer to Web version on PubMed Central for supplementary material.

ACKNOWLEDGEMENTS

We thank the patients and their families for participation. We thank the Yale pediatric and medicine intensive care teams for providing access to patients. We thank the staff of the Yale Center for Genome Analysis for production of exome sequence data. We thank Dr. C. Roy for *CASP1* and *ASC* constructs. Dr. L. Devine for multiplex cytokine detection. This work was supported by: K12HD0141401-10 from NIH-NICHD (to N. R.), U54 HG006504 01 (Yale Center for Mendelian Genomics) to RPL; R01 AI081825 (NIH/NIAID) to BIK; BIK is a BWF Investigator in the Pathogenesis of Infectious Diseases.

REFERENCES

1. Mariathasan S, Monack DM. Inflammasome adaptors and sensors: intracellular regulators of infection and inflammation. Nat Rev Immunol. 2007; 7:31–40. [PubMed: 17186029]
2. Dinarello CA. Immunological and inflammatory functions of the interleukin-1 family. Annu Rev Immunol. 2009; 27:519–50. [PubMed: 19302047]
3. Ozen S, Bilginer Y. A clinical guide to autoinflammatory diseases: familial Mediterranean fever and next-of-kin. Nat Rev Rheumatol. 2014; 10:135–47. [PubMed: 24247370]
4. Thornberry NA, et al. A novel heterodimeric cysteine protease is required for interleukin-1 beta processing in monocytes. Nature. 1992; 356:768–74. [PubMed: 1574116]
5. Miao EA, et al. Cytoplasmic flagellin activates caspase-1 and secretion of interleukin 1beta via Ipaf. Nat Immunol. 2006; 7:569–75. [PubMed: 16648853]
6. Sutterwala FS, et al. Immune recognition of Pseudomonas aeruginosa mediated by the IPAF/NLRC4 inflammasome. J Exp Med. 2007; 204:3235–45. [PubMed: 18070936]
7. Martinon F, Burns K, Tschopp J. The inflammasome: a molecular platform triggering activation of inflammatory caspases and processing of proIL-beta. Mol Cell. 2002; 10:417–26. [PubMed: 12191486]
8. Mariathasan S, et al. Differential activation of the inflammasome by caspase-1 adaptors ASC and Ipaf. Nature. 2004; 430:213–8. [PubMed: 15190255]
9. Broz P, von Moltke J, Jones JW, Vance RE, Monack DM. Differential requirement for Caspase-1 autoproteolysis in pathogen-induced cell death and cytokine processing. Cell Host Microbe. 2010; 8:471–83. [PubMed: 21147462]

10. Miao EA, et al. Caspase-1-induced pyroptosis is an innate immune effector mechanism against intracellular bacteria. Nat Immunol. 2010; 11:1136–42. [PubMed: 21057511]
11. Jordan MB, Allen CE, Weitzman S, Filipovich AH, McClain KL. How I treat hemophagocytic lymphohistiocytosis. Blood. 2011; 118:4041–52. [PubMed: 21828139]
12. Hu Z, et al. Crystal structure of NLRC4 reveals its autoinhibition mechanism. Science. 2013; 341:172–5. [PubMed: 23765277]
13. Hoffman HM, Mueller JL, Broide DH, Wanderer AA, Kolodner RD. Mutation of a new gene encoding a putative pyrin-like protein causes familial cold autoinflammatory syndrome and Muckle-Wells syndrome. Nat Genet. 2001; 29:301–5. [PubMed: 11687797]
14. Agostini L, et al. NALP3 forms an IL-1beta-processing inflammasome with increased activity in Muckle-Wells autoinflammatory disorder. Immunity. 2004; 20:319–25. [PubMed: 15030775]
15. Aksentijevich I, et al. De novo CIAS1 mutations, cytokine activation, and evidence for genetic heterogeneity in patients with neonatal-onset multisystem inflammatory disease (NOMID): a new member of the expanding family of pyrin-associated autoinflammatory diseases. Arthritis Rheum. 2002; 46:3340–8. [PubMed: 12483741]
16. Neven B, Prieur AM, Quartier dit Maire P. Cryopyrinopathies: update on pathogenesis and treatment. Nat Clin Pract Rheumatol. 2008; 4:481–9. [PubMed: 18665151]
17. Fernandes-Alnemri T, et al. The pyroptosome: a supramolecular assembly of ASC dimers mediating inflammatory cell death via caspase-1 activation. Cell Death Differ. 2007; 14:1590–604. [PubMed: 17599095]
18. Man SM, et al. Inflammasome activation causes dual recruitment of NLRC4 and NLRP3 to the same macromolecular complex. Proc Natl Acad Sci U S A. 2014; 111:7403–8. [PubMed: 24803432]
19. Canna S. An activating NLRC4 inflammasome mutation causes a novel autoinflammatory syndrome presenting with recurrent Macrophage Activation Syndrome. Nature Genetics (In revision). 2014
20. Franchi L, et al. NLRC4-driven production of IL-1beta discriminates between pathogenic and commensal bacteria and promotes host intestinal defense. Nat Immunol. 2012; 13:449–56. [PubMed: 22484733]
21. Yatsunenko T, et al. Human gut microbiome viewed across age and geography. Nature. 2012; 486:222–7. [PubMed: 22699611]
22. Lachmann HJ, et al. Use of canakinumab in the cryopyrin-associated periodic syndrome. N Engl J Med. 2009; 360:2416–25. [PubMed: 19494217]
23. Hawkins PN, Lachmann HJ, Aganna E, McDermott MF. Spectrum of clinical features in Muckle-Wells syndrome and response to anakinra. Arthritis Rheum. 2004; 50:607–12. [PubMed: 14872505]
24. Hoffman HM, et al. Efficacy and safety of rilonacept (interleukin-1 Trap) in patients with cryopyrin-associated periodic syndromes: results from two sequential placebo-controlled studies. Arthritis Rheum. 2008; 58:2443–52. [PubMed: 18668535]
25. Bernstein FC, et al. The Protein Data Bank. A computer-based archival file for macromolecular structures. Eur J Biochem. 1977; 80:319–24. [PubMed: 923582]
26. Zaidi S, et al. De novo mutations in histone-modifying genes in congenital heart disease. Nature. 2013; 498:220–3. [PubMed: 23665959]
27. Vijayan D. Isolation and differentiation of monocytes-macrophages from human blood. Methods Mol Biol. 2012; 844:183–7. [PubMed: 22262443]
28. Wangdi T, Mijares LA, Kazmierczak BI. In vivo discrimination of type 3 secretion system-positive and -negative Pseudomonas aeruginosa via a caspase-1-dependent pathway. Infect Immun. 2010; 78:4744–53. [PubMed: 20823203]

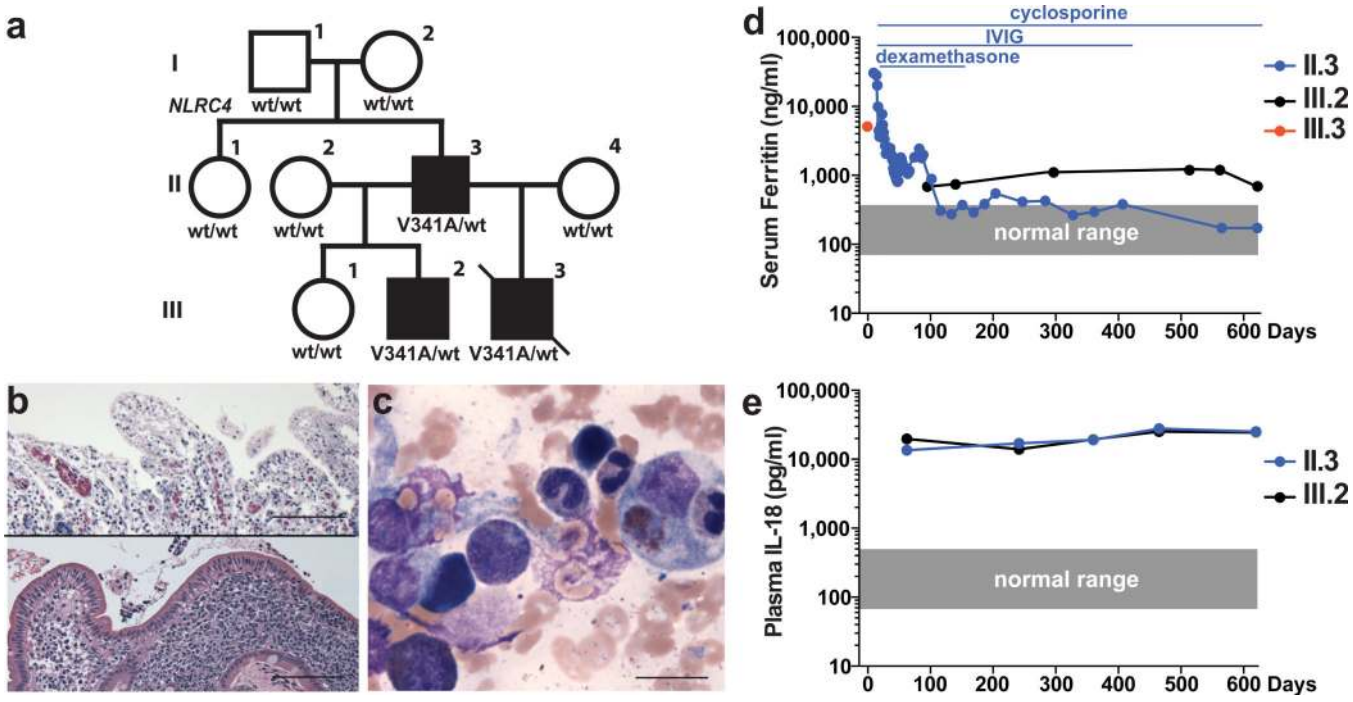

Figure 1.

Kindred with syndrome of infantile enterocolitis and autoinflammation caused by mutation of *NLRC4*. (**a**) Kindred structure. Affected members are denoted by filled symbols. Genotypes at the *NLRC4* locus are indicated. (**b**) Hematoxylin and eosin staining of duodenal tissue obtained by autopsy (upper panel, patient III.3) or biopsy (lower panel, patient III.2) demonstrating villous blunting and intraepithelial lymphocytes. Original magnification 200x. Scale bars, 500 μm (**c**) Hematoxylin and eosin staining of bone marrow from patient II.3 during an episode of acute autoinflammation demonstrating hemo and myelo-phagocytosis. Original magnification 1000x. Scale bar, 20 μm. (**d**) Elevated serum ferritin concentrations in three affected patients. Immune modulatory treatments used in patient II.3 (blue) are indicated. Institutional normal range is indicated in gray. T=0 represents the birth date of subject III.3. The father (II.3) presented with acute illness at day 28. Subject III.2 has been interictal during laboratory assessments and without severe febrile episodes throughout the observed interval. (**e**) Elevated plasma IL-18 in patients II.3 and III. 2. Normal range, indicated in gray, was determined by testing plasma of four related (three adult, one pediatric) and 18 un-related (13 adult, five pediatric) healthy controls.

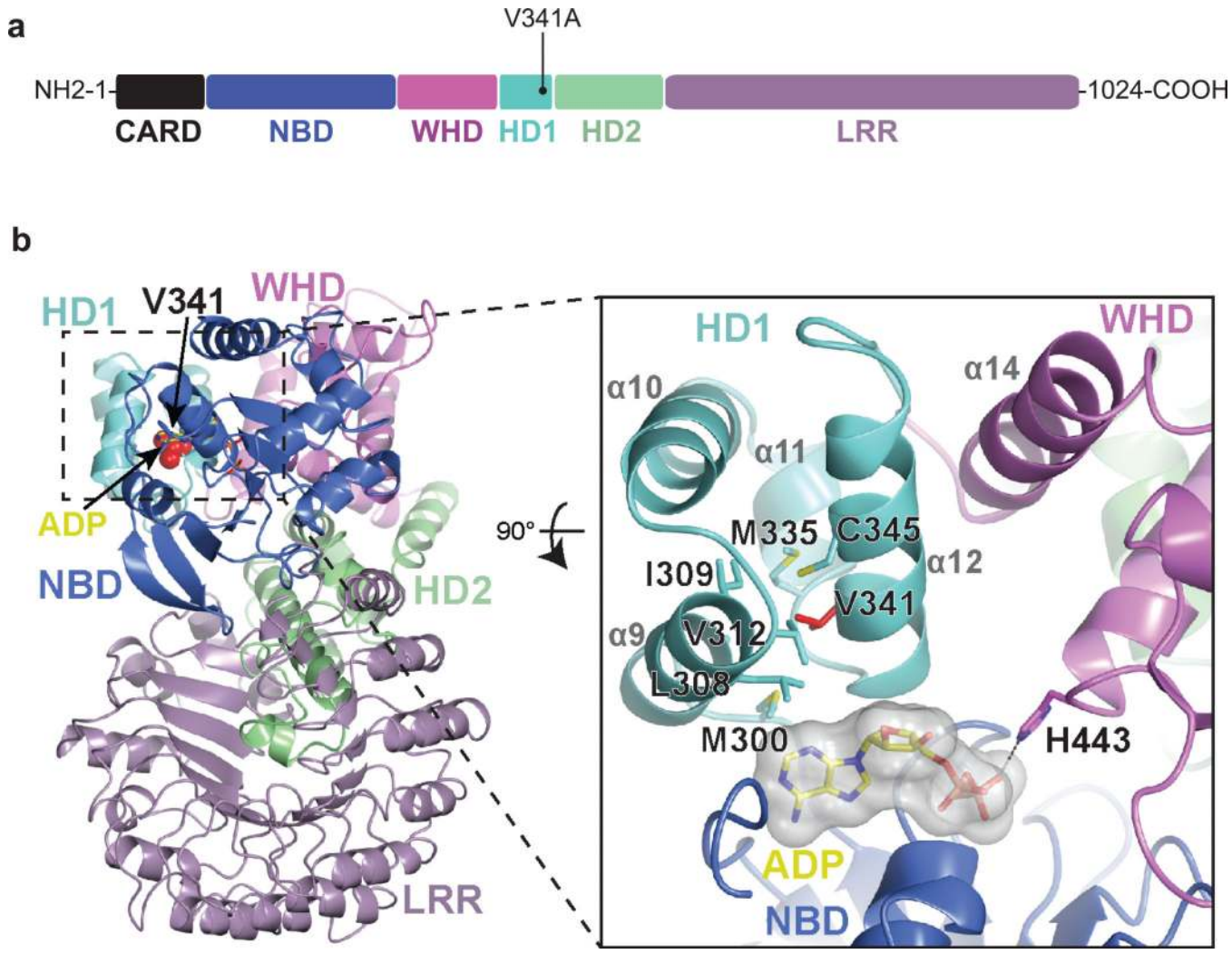

Figure 2.

The V341A amino acid substitution is positioned within the HD1 domain of NLRC4. (**a**) A schematic representation of the NLRC4 protein with individual domains colored as follows: CARD in black, NBD in blue, HD1 in cyan, WHD in pink, HD2 in green, LRR in lilac. The location of the V341A substitution is displayed (**b**) Mapping of Val-341 onto the crystal structure of murine NLRC4 in the ADP-bound state (PDB accession code 4KXF)[12,25]. The ribbon diagram excludes the N-terminal CARD domain which was not included in its crystal structure. ADP is drawn as sticks, and the position of Val-341 is indicated with red spheres. The zoomed-in region (structure rotated 90° toward the reader) shows the position of Val-341 on α–helix 12. Neighboring hydrophobic residues within the HD1 (black outlines) and adjacent α-helices are numbered.

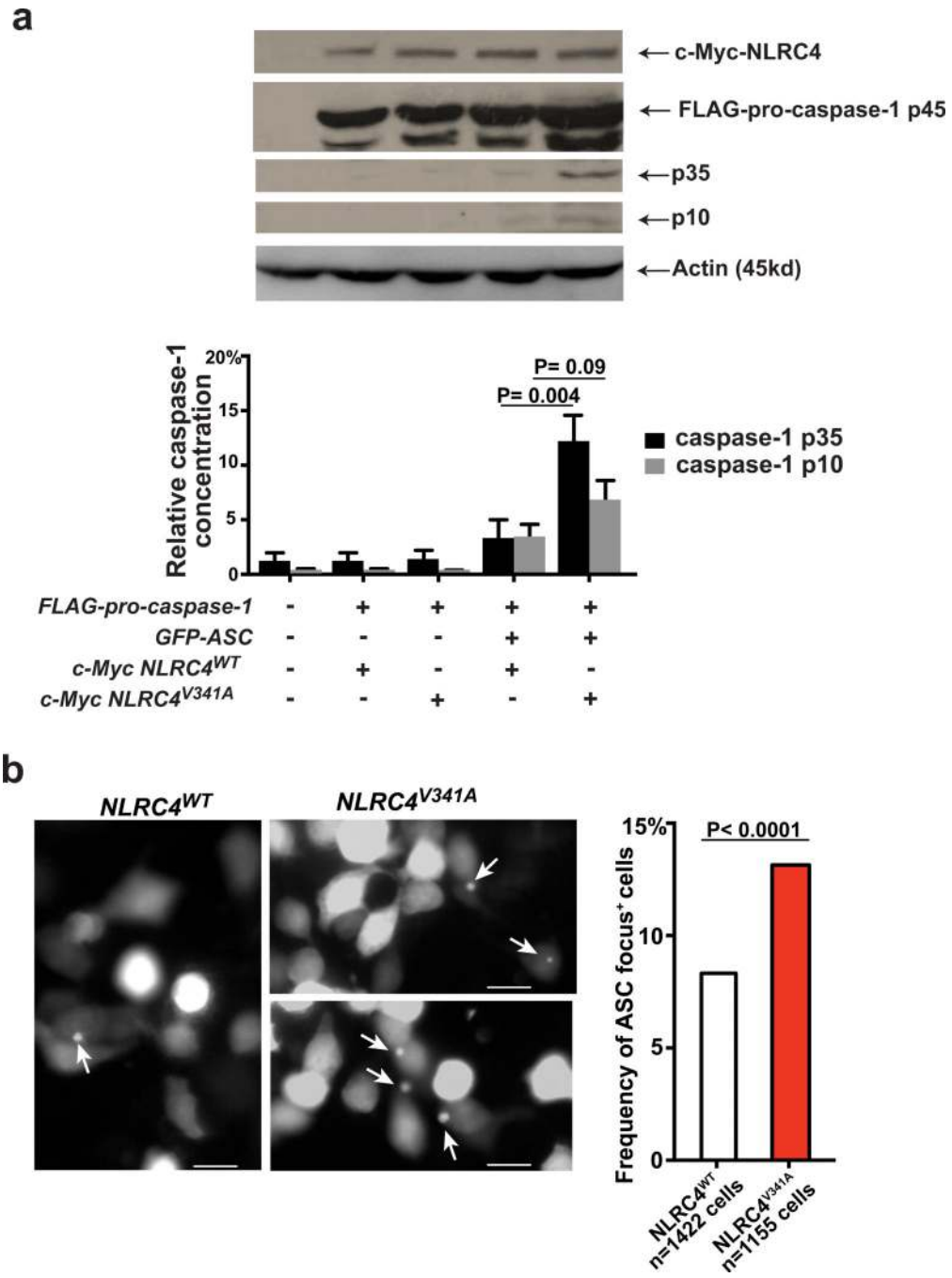

Figure 3.

NLRC4^{V341A} promotes spontaneous cleavage of pro-caspase-1 and ASC multimerization in HEK293 cells. (**a**) Increased cleavage of FLAG-procaspase-1 in HEK293 cells expressing NLRC4^{V341A} versus NLRC4^{WT}. Western blot at top of figure shows results of blotting for NLRC4, pro-caspase-1 (p45) and its p35 and p10 cleavage products as well as actin controls in cells expressing constructs shown below, as described in Methods. Levels of p35 and p10 are normalized in each case to the level of pro-caspase-1. Alternate analysis normalizing p35 and p10 to levels of actin and NLRC4 also yielded statistically significant differences

between lines transfected with *NLRC4*^{WT} and *NLRC4*^{V341A}. Mean and standard deviation of four independent transfections is shown. A two-sided Student's t-test was used to determine statistical significance. (**b**) Spontaneous ASC multimerization (white arrows) in HEK293 cells expressing GFP-ASC and either *NLRC4*^{WT} (left panel) or *NLRC4*^{V341A} (right panels) using epifluorescent microscopy. A total of 1422 cells transfected with wildtype NLRC4 and 1155 cells transfected with mutant NLRC4 were scored. * the frequency of ASC puncta^{+} cells in lines transfected with *NLRC4*^{WT} is significantly different ($P<0.0001$) from lines transfected with *NLRC4*^{V341A} (chi-square testing). Scale bars, 20 μm.

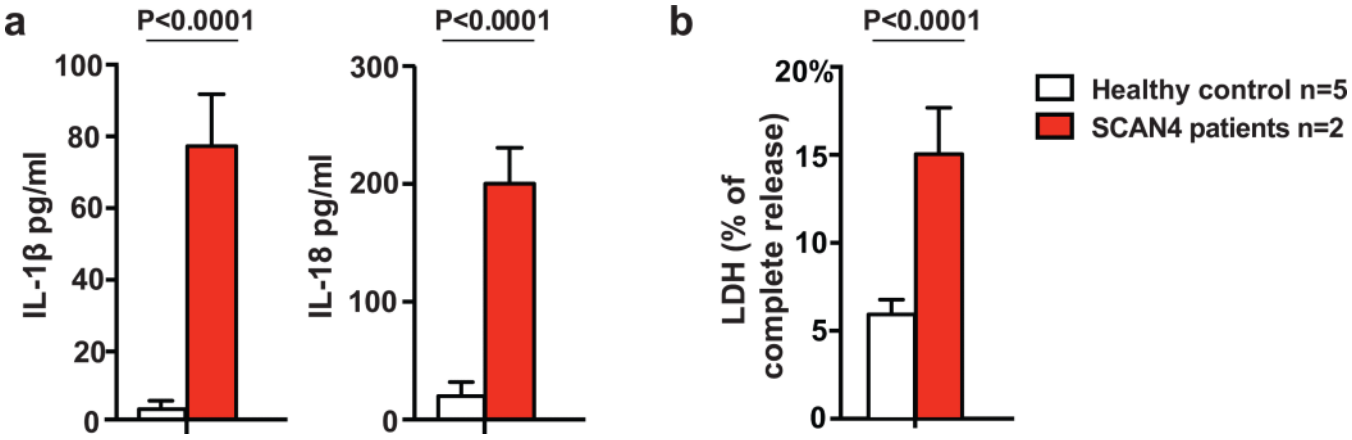

Figure 4.

Increased production of IL-1β,IL-18 and increased cell death in macrophages harboring NLRC4^{V341A}. Monocyte-derived macrophages from SCAN4 patients (II.3 and III.2) and WT controls (one related and four unrelated) were cultured for 18 hours in media containing low-dose LPS (1 ng/ml) followed by measurement of (**a**) IL-1-β(**b**) IL-18, and (**c**) LDH as described in Methods. LDH release is reported relative to result following total lysis by TritonX-100 (0.1%). Cytokine secretion and cell death results were similar in macrophages from patients (II.3 and III.2). Bar graphs show mean ± S.E.M from three separate experiments. Significance by unpaired Student's t-test is indicated.

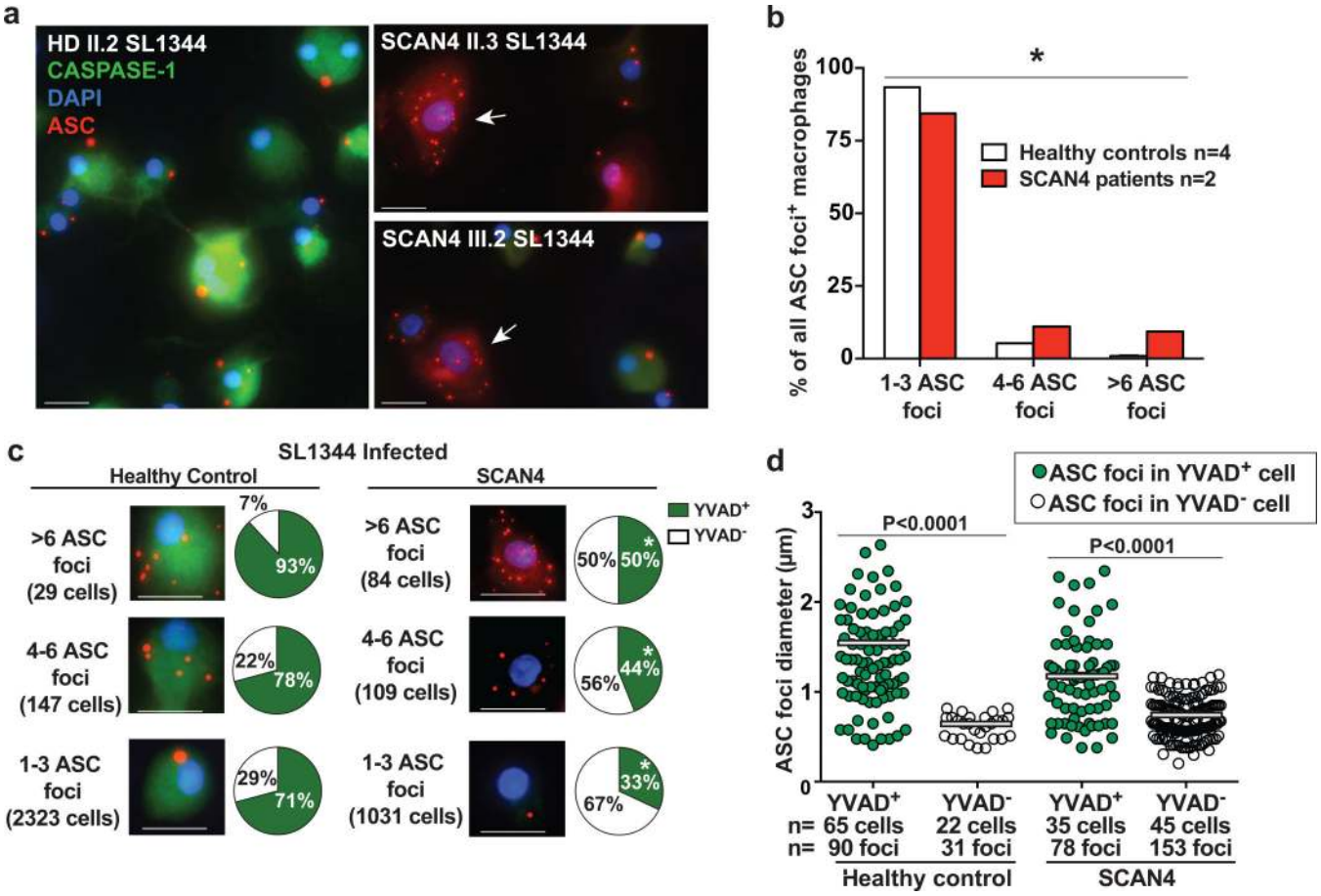

Figure 5.

SCAN4 macrophages infected with *S. typhimurium* strain SL1344 show abnormal ASC staining and limited activation of caspase-1. (a) The majority of *S. typhimurium* infected monocyte-derived macrophages from a representative healthy control (HD II.2, the mother of SCAN4 patient III.2) display features of conventional macrophage activation including biotin-YVAD-CMK staining (green cytoplasm) and a limited number (1-3) of ASC foci (red puncta) per cell (left panel). A subset of *S. typhimurium* infected macrophages (white arrows) from SCAN4 patients II.3 and III.2 display numerous (>6) ASC foci but more limited staining for biotin-YVADCMK (right panel). Scale bars, 20 µm (b) Quantitation of ASC foci in 2499 SL1344 infected healthy control macrophages and 1224 *S. typhimurium* infected patient macrophages. (c) Representative biotin-YVAD-CMK staining in *S. typhimurium* infected healthy control or SCAN4 macrophages from groups with either 1-3, 4-6 or >6 ASC foci/cell. Pie charts display the frequency of biotin-YVAD-CMK positive cells per group. Total cell number analyzed within each group listed within parentheses. Scale bars, 20 µm. (d) Diameter of ASC foci in biotin-YVADCMK positive macrophages (filled green circles) and biotin-YVAD-CMK negative macrophages (unfilled circles) from healthy control and SCAN4 patients II.3 and III.2. Mean foci diameter displayed as white bars. * patient cell distribution is significantly different (P<0.0001) from the healthy control

cell distribution by chi-square statistical testing (for b and c). Significance by unpaired Student's t-test is indicated (for d).